Determination of Atomic-scale Structure and Compressive Behavior of Solidified $Al_xCrCoFeCuNi$ High Entropy Alloys

Mehran Bahramyan, Reza Taherzadeh Mousavian, Dermot Brabazon

I-Form, Advanced Manufacturing Research Centre & Advanced Processing Technology Research Center, School of Mechanical & Manufacturing Engineering, Dublin City University, Dublin 9, Ireland

E-mail addresses: mehran.bahramyan2@mail.dcu.ie (M. Bahramyan), rezataherzadeh.mousavian@dcu.ie (R. Taherzadeh Mousavian), dermot.brabazon@dcu.ie(D. Brabazon).

https://doi.org/10.1016/j.ijmecsci.2019.105389

Abstract

The atomic configurations play a key role in predicting the solidification process of high-entropy alloys (HEAs).The atomic scale structures of $Al_xCrCoFeCuNi$ (x = 0.5, 1.5, 3.0) HEAs that emerge during solidification witha cooling rate of 12×10^9 (K/s) are evaluated using molecular dynamics (MD) simulation. While BCC (body- centered cubic) structure is obtained for $Al_{0.5}CrCoFeCuNi$ and $Al_{1.5}CrCoFeCuNi$ where lattice distortion increases with increasing aluminum fraction from x = 0.5 to x = 1.5, for $Al_{3.0}CrCoFeCuNi$, an amorphous structure is formed under the same cooling rate. The diffusion coefficient of all the elements at 2200 K and the super-heating temperature of each alloy are evaluated to explain the disordering mechanism due to aluminum addition, which affects both the aluminum mobility and diffusion of the constituent atoms in the HEA. Finally, the compression behavior of all the three HEAs was studied to show the effect of crystalline structure on the stress fluctuation. It was found that phase transformation induced plasticity occurred which led to a secondary hardening of crystalline alloys after ultimate compressive strength (UCS).

Introduction

In 2004, a new class of alloys, referred to as high entropy alloy (HEAs), were proposed. HEAs commonly contain more than five elements with equal or near equal molar percent, but crystallize assolid solution, rather than intermetallic, when a suitable cooling rate is applied [1–23]. According to the constituent elements, methods and conditions of fabrication, HEAs with different structures and different number of phases (single-phase or multi-phase) can be synthesized. In single-phase crystalline structures, BCC HEAs exhibit high strength andlow plasticity, while FCC (face-centered cubic) HEAs shows high plasticity and low strength[24]. To overcome the formation of undesirable phases with unsuitable morphology, rapid surface melting with coolingrates as high as 10^6 K/s contrary to $10–10^2$ K/s in conventional casting has been utilized for microstructural refinement, enhanced homogenization, as well as to reduce formation of brittle phases. However, an in-situstudy of microstructural evolution at such high cooling rates, to under- stand how atomic ordering occurs, is a hard task experimentally. One ofthe most extensively investigated HEAs with notable mechanical properties is $Al_xCrCoFeCuNi$ [25–47], where x (the molar ratio in the alloy) ranges from 0 to 3. This alloy has been extensively studied especially to investigate phase formation after casting followed with a normal cooling rate ($10–10^2$ K/s) and after splat quenching with a high cooling rate.

Microstructure characterization of the $Al_xCrCoFeCuNi$ alloy system was reported by Tong et al. (2005) [48]. In that paper it was noted that arc-melting of the elements followed by a normal cooling rate led to the prediction of a phase diagram that showed the occurrence of BCC crystallographic structures by the addition of aluminum. Also, it was found that by increasing the amount of aluminum (x = 0–3), the lattice constant of BCC and especially FCC structure increased. Finally, it was reported that high mixing entropy and sluggish cooperative diffusion enhanced the formation of simple solid-solution phases and submicronic structures with nanoprecipitates in the alloys with multi-principal elements rather than intermetallic compounds. Some studies [49,50] have been reported regarding diffusion kinetics of elements in HEAs, while the effect of sluggish diffusion hypothesis in HEAs is not fully understood. The concurrence of spinodal decomposition and nano-phase precipitation in a AlCrCoFeCuNi high-entropy alloy produced by arc melting, spray casting and melt spinning was investigated by Zhang et al. (2019) [51]. They applied $10^6 – 10^7$ K/s as the high cooling rate forthe melt spinning process which however could not inhibit the spinodaldecomposition and nano-phase precipitation. In fact, three typical struc- tures including Cu-rich nano-precipitates of FCC structure, Al-Ni-rich plate of B2 structure, and Fe-Cr-rich plate of A2 structure were observedand the width of modulated plate decreased with the increase of the cooling rate. Xu et al. (2015) [36] suggested that in $Al_{0.5}CrCoFeCuNi$

HEAs, nano-scale phase separation can effectively minimize the lattice distortions caused by the atomic size difference in the constituent elements, which may offer phase stability of the FCC structure in such alloys. In fact, they reported that complex microstructural evolution occurs in dual-phase HEAs, while in single-FCC phase, HEAs may behave like a traditional FCC metal. Based on the above-mentioned reports, it seems that researchers have focused on a high cooling rate to reduce the detrimental effects of brittle intermetallic phases. Instead, they have reported the advantages of nano-sized precipitate dispersion of intermediate phases and improvement in mechanical properties via increasing the solidification rate even up to 10^7 (K/s) using new techniques such as splat quenching and the selective laser melting process. The difficulty in observing the phase transition of materials at the nanoscale with in-situ experiments promotes the use of powerful computational techniques like MD simulations and ab-initio calculations [1,13,26,34,35,47,52–56]. Sharma et al. (2017) [57] studied the atomic origin of the structural phase transformation in $Al_xCrCoFeNi$. They investigated the role of Al in diffusive transformation from molten to crystalline phase. Zhang et al. (2018) [47] investigated the structural and bonding transformation of $Al_{0.67}CrCoFeNi$ during solidification. They have studied the effect of cooling rate on the type of clusters formed in the HEA. In addition, Li et al [58] reported the effect of cooling rate on proportion of BCC solid solution and amorphous structure in AlCrCoCuFeNi. From the literature to date, it is clear that the effects of Al concentration at the atomic scale on the structure of these solidified HEAs is not well understood and the main aim of this study is to contribute to achieving a more clear understanding of these effects.

For HEAs, phase transformation induced plasticity (TRIP) has been reported during tensile deformation which can cause hardening or softening in the plastic region [59–61]. To the best of the authors knowledge, no attempt has been made to study the compression behavior of HEAs based on TRIP mechanisms at atomic scale. In this study, the cooling rate during the solidification process was examined ranging from 21×10^{12} K/s (Used in [62]) to 12×10^9 K/s to characterize the solidification mechanisms and provide the final microstructure by the addition of aluminum. Results showed that a BCC-based structure with homogeneous distribution of components can be formed with a low concentration of aluminum. Also, the microstructural evolution during solidification of $Al_xCrCoFeCuNi$ and the effect of Al concentration on the final structure of these HEAs after quenching was reported and discussed. Finally, the compressive behavior of crystalline and amorphous structures was evaluated and the occurrence of TRIP during compression test was discussed for the crystalline alloys.

1. Simulation details

Due to the importance of choosing a reliable interatomic potential in MD simulations, EAM (Embedded Atom Method) potential was used for describing the interatomic interaction between Al-Cr-Co-Fe-Cu-Ni, [8,63,64].

In order to check the reliability of the employed EAM potential, the density of the HEAs were calculated and compared with the density obtained from the mixture rule. MD results showed that density of $Al_{0.5}CrCoFeCuNi$ and $Al_{1.5}CrCoFeCuNi$ are 7.6 (g/cm^3) and 6.72 (g/cm^3), respectively, which is in good agreement with the mixture rule results as 7.634 (g/cm^3) and 6.639 (g/cm^3), respectively. The atomic simulation box for the three types of alloys was exposed to the solidification process with a rate of 12×10^9 K/s. The superheating and supercooling temperature were estimated by the change in the slop of simulation box potential energy difference with the temperature in the cooling and heating process. Finally, The uni-axial compression test was then applied along the z direction at the strain rate of $10^{10}\ s^{-1}$. The other simulation details have been provided elsewhere [62].

The dynamics of atoms in three molten HEAs were investigated through calculation of mean square displacement (MSD) and velocity auto-correlation functions (VACF) and self-diffusion coefficients for each species were derived. The M(t) (MSD at time t) could be defined as [54]

$$M(t) = \frac{1}{N}\sum_{i=1}^{N} < (x_i(t) - x_i(0))^2 > \quad (1)$$

where $x_i(t)$ is the position of each atom at time t and N is the total number of atoms. The VACF is another technique to derive the self-diffusion coefficient that can be defined as [54]

$$C(t) = < v_i(t).v_i(t=0) > \quad (2)$$

where $v_i(t)$ is the velocity of atom i at time t and brackets shown an average over time and all the same species of the atoms. Both MSD and VACF can be used to extract the self-diffusion coefficient, D of the molten HEAs. D can be derived from the linear slope of the MSD, as [54]

$$D = \frac{1}{6}\frac{\partial M(t)}{\partial t} = \frac{1}{6}\frac{\partial}{\partial t}\left(\frac{1}{N}\sum_{i=1}^{N} < (x_i(t) - x_i(0))^2 >\right) \quad (3)$$

Also, it is possible to calculate D using time integration of VACF, as [54]

$$D = \frac{1}{3}\int_0^{\infty} C(t)dt \quad (4)$$

The large-scale atomic/molecular massively parallel simulator (LAMMPS) [65] was used for MD simulations and trajectories of atoms were studied using The Open Visualization Tool (OVITO) [66] software. The CNA (Common Neighbor Analysis) [67,68] was used to show the crystal structure of the samples. The X-ray diffraction (XRD) peak profiles was extracted from the LAMMPSUSER-DIFFRACTION package [69,70]. The chosen wavelength was λ = 1.541838 A°.

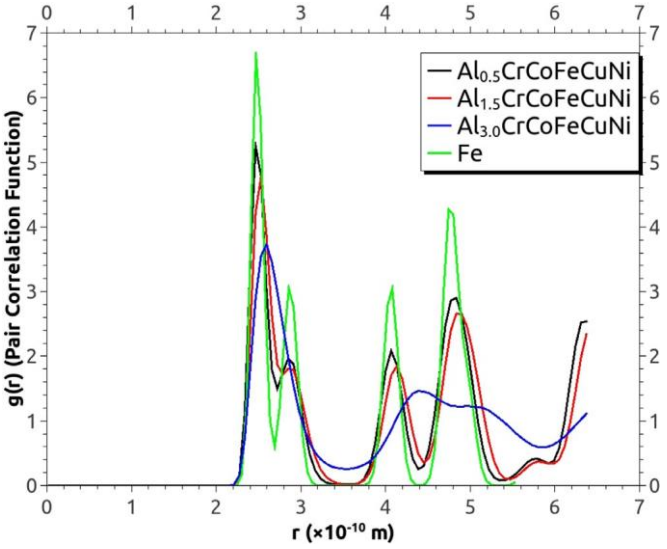

Fig. 1. g(r) of $Al_{0.5}CrCoFeCuNi$, $Al_{1.5}CrCoFeCuNi$ and Fe at 300K.

2. Results and discussion

The pair distribution function (PDF or g(r)) results for the $Al_{0.5}CrCoFeCuNi$, $Al_{1.5}CrCoFeCuNi$ showed strong peaks in some cutoff distances (signature of the BCC structure) which can indicate ordered structure in the sample while g(r) results for $Al_{3.0}CrCoFeCuNi$ showed a disordered structure (see Fig. 1). Occupying the same crystallographic sites by atoms with a different size could lead to the distorted lattice which can affect the microstructure of HEAs. [71]. The whole g(r) of the HEA samples and BCC-Fe as perfect crystal model shows the significant difference especially at the second peak. The strong broadening of the peaks in $Al_{0.5}CrCoFeCuNi$ and $Al_{1.5}CrCoFeCuNi$ compared with the Fe model illustrated that locally lattice distorted away from the average

Table 1
FWHM of the first peaks of the alloys shown in the Fig. 1.

Alloys	FWHM* (*Angstrom*(Å))
$Al_{0.5}CrCoFeCuNi$	0.2388
$Al_{1.5}CrCoFeCuNi$	0.2647
$Al_{3.0}CrCoFeCuNi$	0.4785
Fe	0.1697

* Full Width at Half Maximum

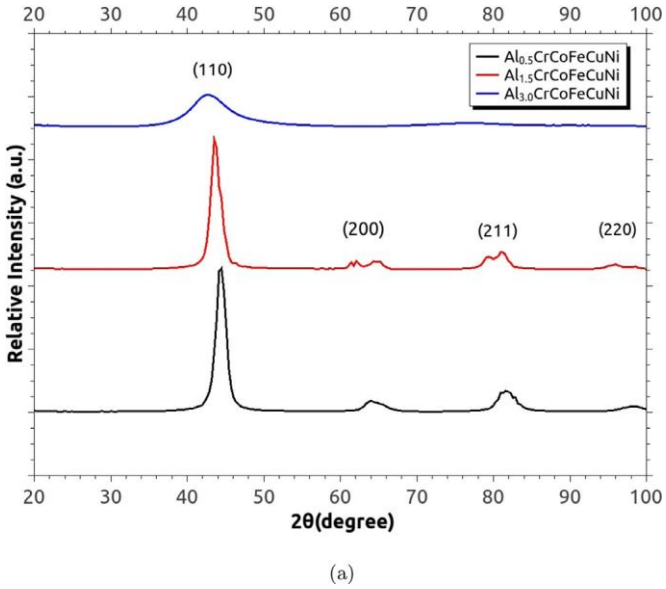

(a)

Fig. 2. a) Full g(r) for $Al_{0.5}CrCoFeCuNi$, $Al_{1.5}CrCoFeCuNi$ and $Al_{3.0}CrCoFeCuNi$. b) X-ray Diffraction peak profile of BCC phase of $Al_{0.5}CrCoFeCuNi$, $Al_{1.5}CrCoFeCuNi$ and $Al_{3.0}CrCoFeCuNi$.

BCC structure (Fe) in these HEAs. Owen et al. [72] reported that broader PDF peaks in HEAs could suggest the highest level of local lattice strain within the materials studied. In order to compare the broadening of the first peaks, full width at half maximum (FWHM) of the peaks from Gaussian fits were obtained and tabulated in the Table 1. From the results, it can be concluded that lattice distortion in $Al_{1.5}CrCoFeCuNi$ is a little higher than $Al_{0.5}CrCoFeCuNi$ due to the broader peaks of this alloy. These results are in good agreement with the experimental results showing that $Al_{0.5}CrCoFeCuNi$ has a distorted lattice and addition of Al could cause a more distorted structure [26,71,73].

The XRD results as shown in the Fig. 2, illustrate the phase analysis of the solidified alloys. As can be seen, there is a strong texture for (110) planes of BCC structure for $Al_{0.5}CrCoFeCuNi$ and $Al_{1.5}CrCoFeCuNi$ almost with the same peak intensity between these two alloys. However, for (200), (211) and (220) planes, there are some mismatch between $Al_{0.5}CrCoFeCuNi$ and $Al_{1.5}CrCoFeCuNi$. In another experimental study [74], both $Al_{0.5}CrCoFeCuNi$ and $Al_{1.5}CrCoFeCuNi$ were prepared by vacuum arc melting followed by a high rate of solidification where a higher peak intensity was obtained for the (110) crystal texture compared with the other peaks. Also, a slight peak shift towards the lower angles are observed from $Al_{0.5}CrCoFeCuNi$ to $Al_{3.0}CrCoFeCuNi$. These peak shifting can be the consequence of enlarging the lattice constant by the addition of Al atoms as tabulated in Table 2. The size of simulation box after solidification was increased by increasing the number of Al atoms. It can be seen that the volume change from $x = 0.5$ to $x = 1.5$ was around 4.23% while a considerable volume change of 14% was obtained from $x = 0.5$ to $x = 3.0$.

Table 2
The simulation box size of all the samples after the solidification process.

Alloys	x	y (*nm*)	z (*nm*)	Volume (*nm*)	Volume (nm^3)	VC*
CrCoFeCuNi		7.271	7.271	18.179	961.077	–
$Al_{1.5}CrCoFeCuNi$		7.372	7.372	18.432	1001.712	+4.228
$Al_{3.0}CrCoFeCuNi$		7.596	7.596	18.99	1095.708	+14.008

* Volume Change relative to $Al_{0.5}CrCoFeCuNi$

The CNA results illustrated that no apparent elemental segregation can be found in the samples proving the uniform distribution of the HEA models. These results were interesting compared with the results of Zhang et al. (2019) [51] where they applied a high cooling rate and found a mixture of three typical structures including Cu-rich nano-precipitates of FCC structure, Al-Ni-rich plate of B2 structure, and Fe-Cr-rich plate of A2 structure. The CNA Results showed that about 97% and 96% of atoms were in BCC structure for $Al_{0.5}CrCoFeCuNi$ and $Al_{1.5}CrCoFeCuNi$ respectively which is in agreement with the recent study of Li et al. (2019) [75] for AlCrCoFeCuNi alloy. The nucleation and growth of BCC phase during solidification is shown in Fig. 3 for $Al_{1.5}CrCoFeCuNi$. In $Al_{3.0}CrCoFeCuNi$ about 99% of atoms were in other unknown category and no considerable FCC, BCC, HCP (hexagonal close-packed) or icosahedral structures in the sample were found. This difference in crystal structure by rising the molar ratio of Al content could be due to the difficulty in atomic mobilities as atomic radius of Al is bigger than the other elements (see Table 3). The effect of larger atomic size of the Al on the structure of the HEAs have been reported in some studies [55,57,76]. For example, Sharma et al. (2017) [57] reported that increasing the Al concentration in $Al_xCrCoFeNi$ above the equiatomic percentage strongly triggers the glassy structure after solidification. According to the reports of Li et al. (2008) [76] and Yeh et al. (2004) [74], addition of Al as a BCC stabilizer to HEAs can facilitate the formation of BCC phase, while Bonisch et al. (2018) [77] and Tung et al. [73] reported that elements like Fe, Ni, Co and Mn could form HEAs with a FCC structure.

From the above results, $Al_{0.5}CrCoFeCuNi$ and $Al_{1.5}CrCoFeCuNi$ can be classified as crystalline HEAs with true mixing of the 6 elements in BCC structure, indicating the importance of applying the high cooling rates.

To obtain supercooling and superheating temperatures, the variation of the average potential energy of each atom as a function of temperature were determined during solidification and heating processes. As the temperature decreases in the cooling process, the potential energy is decreased and the transition temperature as the supercooling temperature could be evaluated from the deviation of the potential energy from its linear relationship with the temperature[78,79]. Here, the changes of the potential energy versus temperature during cooling and heating processes with the cooling and heating rate of 12×10^9 K/s and 10×10^{12} K/s respectively, were plotted for all the samples with different Al concentrations as shown in the Fig. 4. As can be seen, a sudden reduction occurred in $Al_{0.5}CrCoFeCuNi$ and $Al_{1.5}CrCoFeCuNi$ where an amorphous structure changed to a BCC structure. The extracted superheating and supercooling temperatures are listed in Table 4.

The calculated MSD of the molten HEAs (2200K) are shown in the Fig. 5 and the diffusion coefficient extracted from the slope of these curves according to the Eqs. 3. This increase in the slope of the curves by the addition of Al shows a rise in diffusion coefficient. The extracted diffusion coefficient from the MSD and VACF of HEAs at their superheat temperatures and also 2200 K are available in Table 5. As can be clearly seen, there is a good agreement between the results of both techniques. In addition, the self-diffusion coefficient of each species was extracted using VACF analysis for HEAs with different molar ratio of Al and listed in Table 5. As the results show, both the methods give almost the same outcomes that increasing in Al concentration can lead to a larger diffu-

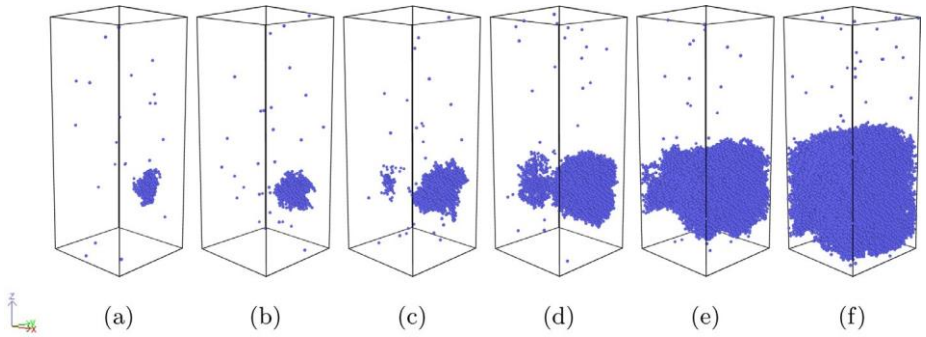

Fig. 3. Snapshots of atomic configuration during nucleation and growth of BCC phase in $Al_{1.5}CrCoFeCuNi$ at temperature around 881K a)111 ns(nanosecond) b)111.04 ns c)111.08 ns d)111.12 ns e)111.16 ns and f)111.2 ns after the quenching process.(Only BCC atoms are shown for clarity).

Table 3
Atomic radiuses of each elements used in interatomic potential.

Elements	Al	Cr	Co	Fe	Cu	Ni
Atomic radius ($\times 10^{-10}$m)	1.43	1.24	1.25	1.24	1.27	1.24
Mass (a.m.u)	26.982	51.996	58.933	55.845	63.546	58.693

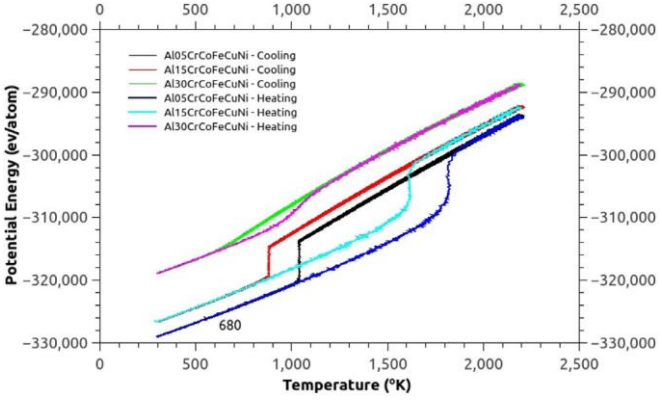

Fig. 4. Potential energy per atom as a function of temperature during the simulated quenching and heating process to estimate the value of supercooling and superheating temperatures at all samples.

Table 4
Estimated superheating and supercooling temperature of all the samples.

	Superheating Temp(K)	Supercooling Temp(K)
$Al_{0.5}CrCoFeCuNi$	1800	1040
$Al_{1.5}CrCoFeCuNi$	1600	880
$Al_{3.0}CrCoFeCuNi$	1000	700

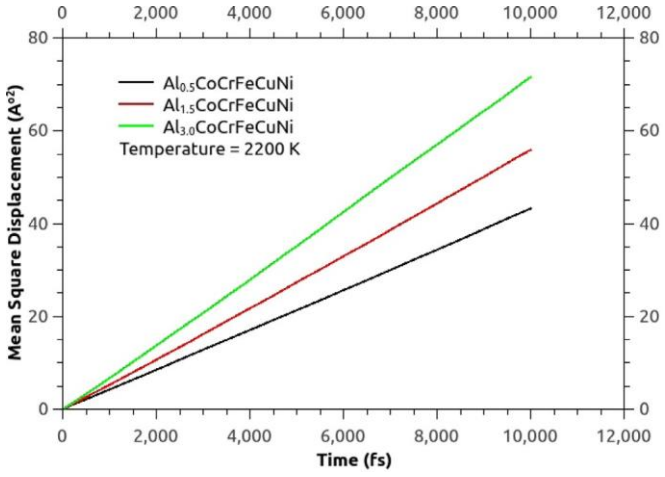

Fig. 5. MSD for $Al_{0.5}CrCoFeCuNi$, $Al_{1.5}CrCoFeCuNi$ and $Al_{3.0}CrCoFeCuNi$ at 2200K .

sion coefficient at 2200K since at this high temperature, light aluminum atoms might have a higher mobility. As can be seen in Table 3, although, the atomic radii of the Al atoms is higher (about 14%), its mass is lower (about 50%) than the other elements. It seems that atoms with a FCC structure (Al, Cu and Ni) have a larger diffusion coefficient compared with the atoms with a BCC structure (Fe and Cr). The high mobility of

Table 5
Diffusion coefficients for HEAs and all species at different temperatures.

		Temp (K)	D(MSD)	D(VACF)	D_{Al}	D_{Co}	D_{Cr}	D_{Fe}	D_{Cu}	D_{Ni}
HEA($Al_{0.5}$)		2200	0.715	0.68	0.87	0.65	0.55	0.622	0.77	0.725
		1800	0.42	0.41	0.56	0.43	0.36	0.365	0.46	0.365
	Reduction	22%↓	70%↓	65%↓	55%↓	51%↓	52%↓	70%↓	67%↓	98%↓
HEA($Al_{1.5}$)		2200	0.91	0.89	0.915	0.96	0.734	0.745	1.0	0.965
		1600	0.395	0.39	0.405	0.36	0.32	0.36	0.46	0.41
	Reduction	37.5%↓	130%↓	128%↓	125%↓	166%↓	129%↓	106%↓	117%↓	135%↓
HEA($Al_{3.0}$)		2200	1.16	1.19	1.33	1.15	0.98	1.0	1.26	1.15
		1000	0.097	0.082	0.108	0.075	0.065	0.075	0.06	0.058
	Reduction	120%↓	1095%↓	1351%↓	1131%↓	1433%↓	1407%↓	1233%↓	2000%↓	1882%↓

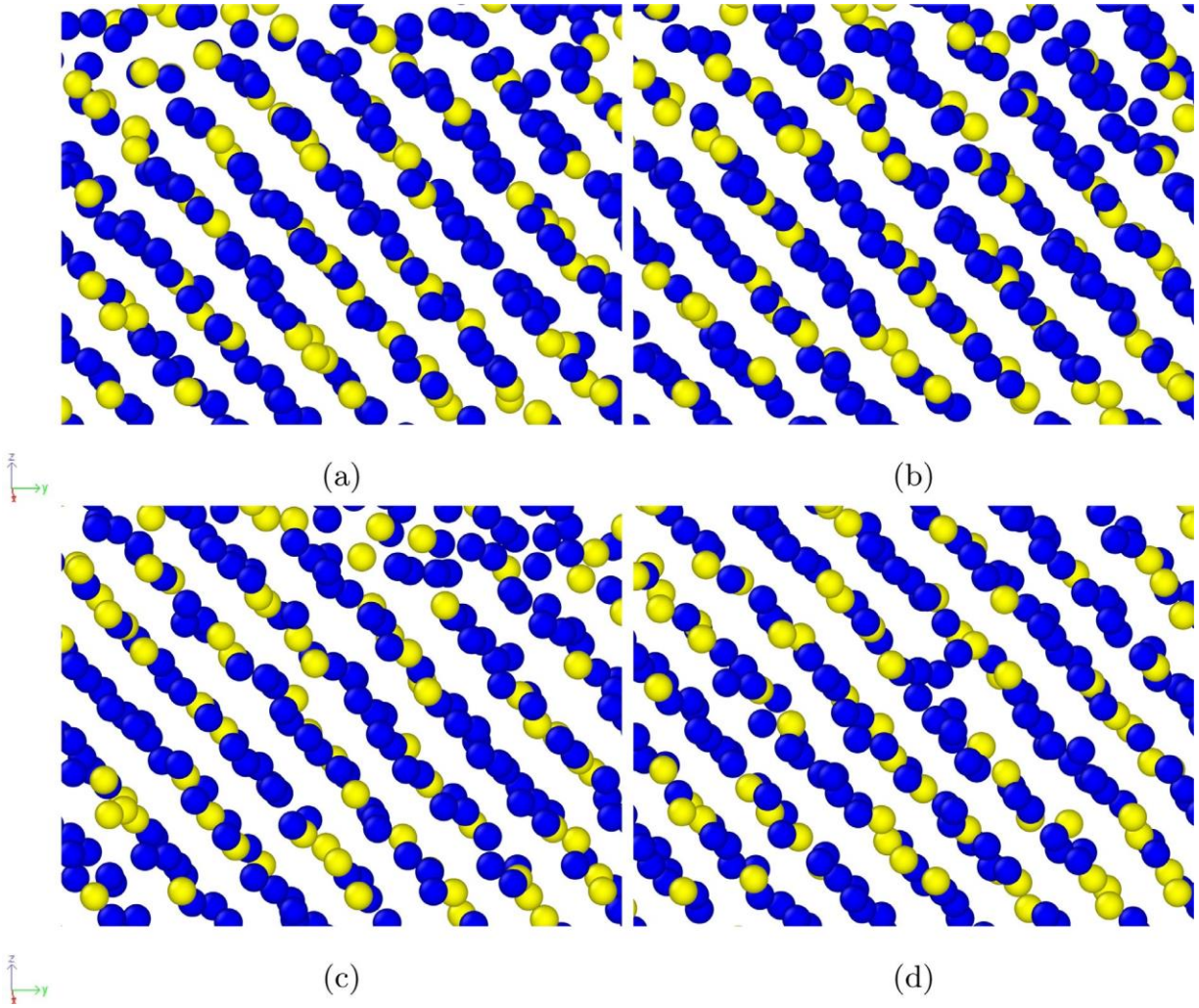

Fig. 6. Al mobility during solidification in $Al_{1.5}CrCoFeCuNi$ at temperature around 881K a)111.08 ns b)111.12 ns c)111.16 ns d)111.2 ns after the quenching process. The yellow colored atoms represent Al atoms while blue color associated to the other atoms. (The movie of these snapshots from different perspective is available in the online version of the article). (For interpretation of the references to color in this figure legend, the reader is referred to the web version of this article.)

Al atoms can be seen in the samples with 0.5 and 3.0 in molar ratio of Al. In $Al_{1.5}CrCoFeCuNi$, Cu atoms showed a higher mobility almost in good agreement with the ab-initio calculation of $Al_{1.3}CrCoFeCuNi$ in [26,80]. This high diffusion rate for Cu may facilitate its precipitation from the matrix, as observed in Santodonato et al. (2015) [26] study in $Al_{1.3}CrCoFeCuNi$ and Zhang et al. (2019) [51] study in AlCrCoFeCuNi. The mobility of Al atoms is shown in the Fig. 6 for $Al_{1.5}CrCoFeCuNi$ at temperature around 881K which shows changing the position of the Al atoms (yellow colored one) during the solidification. The main important outcome from Table 5 is that the addition of aluminum will highly reduce the super-heating temperature and more interestingly, for $x = 3$, a higher reduction in mobility of the other atoms occurred compared with that of aluminum itself that might affect the lack of structure obtained in the CNA analyses. In fact, the presence of aluminum by reducing the super-heating temperature will cause a sharp reduction in mobility of the other atoms especially copper and nickel ones that finally lead to formation of an amorphous structure for $x = 3$.

Fig. 7 shows the compressive behavior of the current HEAs with crystalline and amorphous structure. A lower stress was recorded for the amorphous structure of the $Al_{3.0}CrCoFeCuNi$ and also no fluctuation after UCS was observed for this alloy. A highest stress level at the initial stages of plastic deformation was obtained for the $Al_{0.5}CrCoFeCuNi$, in which a secondary hardening was found after the UCS. Also, for the $Al_{1.5}CrCoFeCuNi$ a similar behavior was recorded while at the start of deformation a negative stress was obtained, indicating that the box

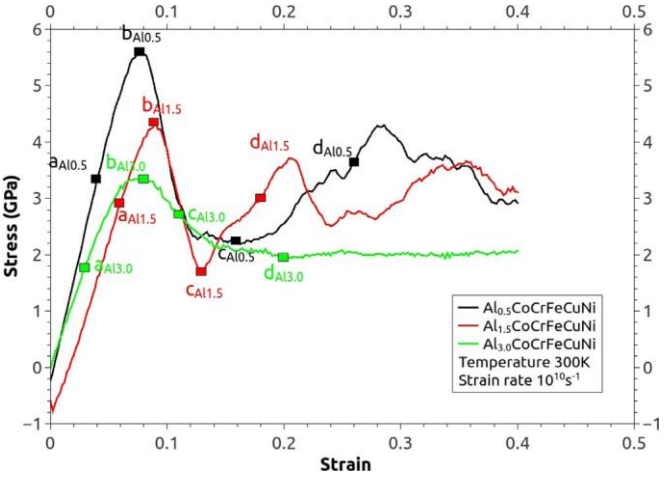

Fig. 7. Compression test results for $Al_{0.5}CrCoFeCuNi$, $Al_{1.5}CrCoFeCuNi$ and $Al_{3.0}CrCoFeCuNi$ at 300K and strain rate of 10^{10}.

was in the negative stress state at the start of compression. In order to find the root cause of secondary hardening for the $Al_{0.5}CrCoFeCuNi$ and the $Al_{1.5}CrCoFeCuNi$, in-situ microstructural characterization was performed and the results were provided in Fig. 8. For this purpose, four points were assigned on the stress–strain curves.

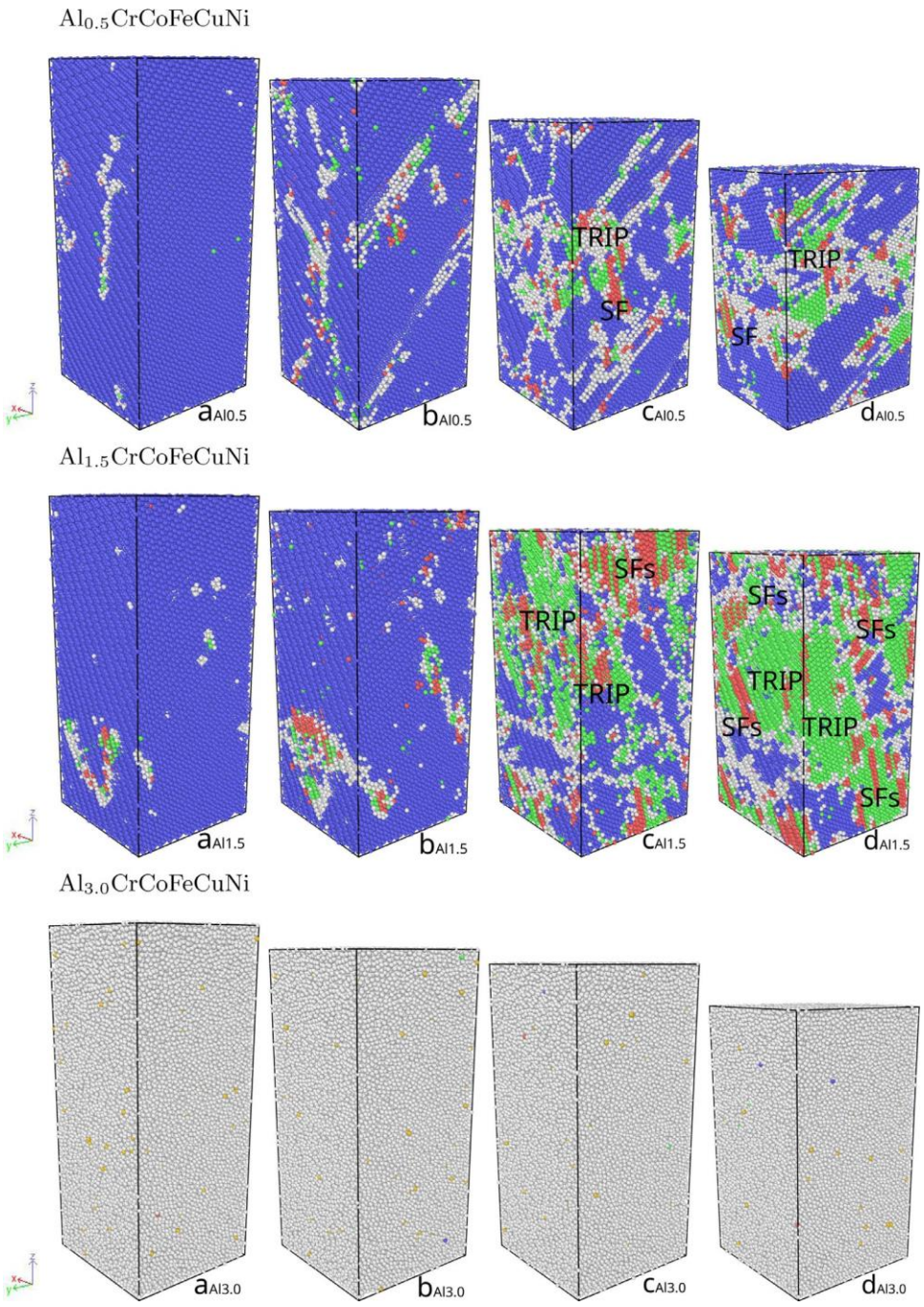

Fig. 8. CNA results during compression test at points illustrated in the Fig. 7 for $Al_{0.5}CrCoFeCuNi$, $Al_{1.5}CrCoFeCuNi$ and $Al_{3.0}CrCoFeCuNi$. In the CNA analysis, each atom is colored for identification of atomic structures as blue for BCC atoms, green for FCC atoms, red for HCP atoms and white for others unknown categories. (For interpretation of the references to color in this figure legend, the reader is referred to the web version of this article.)

The first row of Fig. 8 shows four snapshots for point $a_{Alo.5}$, $b_{Alo.5}$, $c_{Alo.5}$ and $d_{Alo.5}$. As can be seen, by the start of plastic deformation, a phase transformation from BCC structure (blue area) to the other phases occurred during compression. It is interesting that at point $c_{Alo.5}$ where can be considered for the start of hardening, a higher phase transformation was recorded and point $d_{Alo.5}$ demonstrates the highest phase transformation and lowest amount of the BCC structure. Similarly, for $Al_{1.5}CrCoFeCuNi$, the same trend (second row) was obtained, showing the occurrence of TRIP. It should be mentioned that stacking faults (SFs) were detected as HCP structure inside FCC structure. Previous report [81] indicated the considerable effect of the stacking faults formation on the hardening of high entropy alloys. Therefore, it can be concluded that the compressive behavior of high entropy alloys can be influenced by the TRIP mechanism specially when stacking faults can be formed as a result of the phase transformation. Finally, no considerable change in CNA results (third row) was detected for amorphous structure of $Al_{3.0}CrCoFeCuNi$ in which no fluctuation was recorded after UCS.

Conclusions

The solidification behavior of $Al_xCrCoFeCuNi$ HEAs from 2200 K to300 K was investigated in this study. In addition, the compressive behavior of the solidified alloys was investigated. From the simulation results,the following conclusions can be drawn:

1. The RDF results, XRD and CNA analyses indicated that the additionof Al at a molar ratio of 3.0 could lead to an amorphous structure due to the reduced mobility of other atoms. Also, A strong textureof (110) was obtained for crystalline alloys after the solidification which is in agreement with experimental results.

2. The distribution of elements depicted that no phase segregation was formed after solidification which could be due to the higher cooling rate (12×10^9 K/s).

3. MSD and VACF analyses were used for diffusion coefficient derivation and acceptable agreement in extracted results were shown. Theyshowed that increasing in Al concentration results in higher diffusion coefficients of all the elements at 2200K.

4. It was obtained that the addition of aluminum, highly reduces the super-heating temperature of HEA and therefore, the mobility of the other atoms especially nickel and copper will be sharply reduced that causes the formation of an amorphous structure for $x = 3$ in this study.

5. The compressive stress–strain curves indicated that a secondary hardening can be observed for HEAs due to the TRIP mechanism and formation of SFs. It was found that crystalline alloys of this study has a higher UCS compared with amorphous structures.

In future work, super-fast solidification behavior of other types of HEAs with almost the same melting temperature of elements will be studied and validated in experiment to prepare a homogeneous single-phase HEA with a focus on FCC (HCP) structure and a low or negative stacking fault energy (SFE).

Declaration of Competing Interest

The authors declare that they do not have any financial or nonfinancial conflict of interests.

Credit authorship contribution statement

Mehran Bahramyan: Methodology, Software, Writing - original draft.

Reza Taherzadeh Mousavian: Conceptualization, Investigation, Writing - review & editing.

Dermot Brabazon: Supervision, Writing - review & editing.

Acknowledgments

Special thanks should be given to The Irish Centre for High-End Computing (ICHEC) for providing required facilities and high-performance computers. We are also grateful to Dr. Ganesh Balasubramanian from Lehigh University for assistance with discussion of the results.

This research is partially supported by a research grant from Science Foundation Ireland (SFI) under Grant Number 16/RC/3872 and is co-funded under the European Regional Development Fund.

Supplementary material

Supplementary material associated with this article can be found, in the online version, at 10.1016/j.ijmecsci.2019.105389

References

[1] Zhang Y, Zuo TT, Tang Z, Gao MC, Dahmen KA, Liaw PK, et al. Microstructures and properties of high-entropy alloys. Prog Mater Sci 2014;61:1–93. doi:10.1016/j.pmatsci.2013.10.001.

[2] Munitz A, Edry I, Brosh E, Derimow N, MacDonald B, Lavernia E, et al. Liquid phase separation in AlCrFeNiMo 0.3 high-entropy alloy. Intermetallics 2019;112:106517. doi:10.1016/j.intermet.2019.106517.

[3] Liu G, Liu L, Liu X, Wang Z, Han Z, Zhang G, et al. Microstructure and mechanical properties of al0. 7CoCrFeNi high-entropy-alloy prepared by directional solidification. Intermetallics 2018;93:93–100. doi:10.1016/j.intermet.2017.11.019.

[4] Patriarca L, Ojha A, Sehitoglu H, Chumlyakov Y. Slip nucleation in single crystal FeNiCoCrMn high entropy alloy. Scr Mater 2016;112:54–7. doi:10.1016/j.scriptamat.2015.09.009.

[5] Huang J-C. Evaluation of tribological behavior of Al-Co-Cr-Fe-Ni high entropy alloy using molecular dynamics simulation. Scanning 2012;34(5):325–31. doi:10.1002/sca.21006.

[6] Huang E-W, Yu D, Yeh J-W, Lee C, An K, Tu S-Y. A study of lattice elasticity from low entropy metals to medium and high entropy alloys. Scr Mater 2015;101:32–5. doi:10.1016/j.scriptamat.2015.01.011.

[7] Smith T, Hooshmand M, Esser B, Otto F, McComb D, George E, et al. Atomic-scale characterization and modeling of 60° dislocations in a high-entropy alloy. Acta Mater 2016;110:352–63. doi:10.1016/j.actamat.2016.03.045.

[8] Anand G, Goodall R, Freeman CL. Role of configurational entropy in body-centred cubic or face-centred cubic phase formation in high entropy alloys. Scr Mater 2016;124:90–4. doi:10.1016/j.scriptamat.2016.07.001.

[9] Wang Z, Gao M, Ma S, Yang H, Wang Z, Ziomek-Moroz M, et al. Effect of cold rolling on the microstructure and mechanical properties of $Al_{0.25}$ $CoCrFe_{1.25}$ $Ni_{1.25}$ high-entropy alloy. Mater Sci Eng 2015;645:163–9. doi:10.1016/j.msea.2015.07.088.

[10] Tang Z, Senkov ON, Parish CM, Zhang C, Zhang F, Santodonato LJ, et al. Tensile ductility of an AlCoCrFeNi multi-phase high-entropy alloy through hot isostatic pressing (HIP) and homogenization. Mater Sci Eng 2015;647:229–40. doi:10.1016/j.msea.2015.08.078.

[11] Lin C-M, Tsai H-L. Evolution of microstructure, hardness, and corrosion properties of high-entropy $Al_{0.5}$ CoCrFeNi alloy. Intermetallics 2011;19(3):288–94. doi:10.1016/j.intermet.2010.10.008.

[12] Munitz A, Salhov S, Hayun S, Frage N. Heat treatment impacts the micro-structure and mechanical properties of AlCoCrFeNi high entropy alloy. J Alloy Compd 2016;683:221–30. doi:10.1016/j.jallcom.2016.05.034.

[13] Dabrowa J, Kucza W, Cieslak G, Kulik T, Danielewski M, Yeh J-W. Interdiffusion in the FCC-structured Al-Co-Cr-Fe-Ni high entropy alloys: experimental studies and numerical simulations. J Alloy Compd 2016;674:455–62. doi:10.1016/j.jallcom.2016.03.046.

[14] Licavoli JJ, Gao MC, Sears JS, Jablonski PD, Hawk JA. Microstructure and mechanical behavior of high-Entropy alloys. J Mater Eng Perform 2015;24(10):3685–98. doi:10.1007/s11665-015-1679-7.

[15] Gludovatz B, Hohenwarter A, Catoor D, Chang EH, George EP, Ritchie RO.A fracture-resistant high-entropy alloy for cryogenic applications. Science 2014;345(6201):1153–8. doi:10.1126/science.1254581.

[16] Zou Y, Maiti S, Steurer W, Spolenak R. Size-dependent plasticity in an Nb_{25} Mo_{25} Ta_{25} W_{25} refractory high-entropy alloy. Acta Mater 2014;65:85–97. doi:10.1016/j.actamat.2013.11.049.

[17] Anmin L, Zhang X. Thermodynamic analysis of the simple microstructure of AlCrFeNiCu high-entropy alloy with multi-principal elements. Acta Metall Sin 2009;22(3):219–24. doi:10.1016/S1006-7191(08)60092-7.

[18] Ma S, Jiao Z, Qiao J, Yang H, Zhang Y, Wang Z. Strain rate effects on the dynamic mechanical properties of the $AlCrCuFeNi_2$ high-entropy alloy. Mater Sci Eng 2016;649:35–8. doi:10.1016/j.msea.2015.09.089.

[19] Tasan CC, Deng Y, Pradeep KG, Yao M, Springer H, Raabe D. Composition dependence of phase stability, deformation mechanisms, and mechanical properties of the cocrfemnni high-entropy alloy system. JOM 2014;66(10):1993–2001. doi:10.1007/s11837-014-1133-6.

[20] Shun T-T, Du Y-C. Age hardening of the $Al_{0.3}CoCrFeNiC_{0.1}$ high entropy alloy. JAlloyCompd 2009;478(1):269–72. doi:10.1016/j.jallcom.2008.12.014.

[21] Jinhong P, Ye P, Hui Z, Lu Z. Microstructure and properties of $AlCrFeCuNi_x$ ($0.6 \le X \le 1.4$) high-entropy alloys. Mater Sci Eng 2012;534:228–33. doi:10.1016/j.msea.2011.11.063.

[22] Ma SG, Chen ZD, Zhang Y. Evolution of microstructures and properties of the Al_x $CrCuFeNi_2$ high-entropy alloys. In: Materials science forum, 745. Trans Tech Publ; 2013. p. 706–14. doi:10.4028/www.scientific.net/MSF.745-746.706.

[23] Wani I, Bhattacharjee T, Sheikh S, Lu Y, Chatterjee S, Bhattacharjee P, et al. Ultrafine-grained $AlCoCrFeNi_{2.1}$ eutectic high-entropy alloy. Mater Res Lett 2016;4(3):174–9. doi:10.1080/21663831.2016.1160451.

[24] Basu I, Ocelík V, De Hosson JTM. Size effects on plasticity in high-entropy alloys. J Mater Res 2018;33(19):3055–76. doi:10.1557/jmr.2018.282.

[25] Wang S. Paracrystalline property of high-entropy alloys. AIP Adv 2013;3(10):102105. doi:10.1063/1.4824623.

[26] Santodonato LJ, Zhang Y, Feygenson M, Parish CM, Gao MC, Weber RJ, et al. Deviation from high-entropy configurations in the atomic distributions of a multi-principal-element alloy. NatCommun 2015;6. doi:10.1038/ncomms6964.

[27] Chung-Jin T, Min-Rui C, Chen S-K, Yeh J-W, et al. Mechanical performance of the Al_x CoCrCuFeNihigh-Entropy alloy system with multiprincipal elements. Metall Mater Trans 2005;36(5):1263. doi:10.1007/s11661-005-0218-9.

[28] Tsai C-W, Tsai M-H, Yeh J-W, Yang C-C. Effect of temperature on mechanical properties of $Al_{0.5}$ CoCrCuFeNi wrought alloy. J Alloy Compd 2010;490(1):160–5. doi:10.1016/j.jallcom.2009.10.088.

[29] Manzoni A, Daoud H, Mondal S, Van Smaalen S, Völkl R, Glatzel U, et al. Investigation of phases in Al_{23} Co_{15} Cr_{23} Cu_8 Fe_{15} Ni_{16} and Al_8 Co_{17} Cr_{17} Cu_8 Fe_{17} Ni_{33} high en-tropy alloys and comparison with equilibrium phases predicted by thermo-Calc. J Alloy Compd 2013;552:430–6. doi:10.1016/j.jallcom.2012.11.074.

[30] Shaysultanov D, Stepanov N, Kuznetsov A, Salishchev G, Senkov O. Phase composition and superplastic behavior of a wrought AlCoCrCuFeNi high-entropy alloy. JOM 2013;65(12):1815–28. doi:10.1007/s11837-013-0754-5.

[31] Xie L, Brault P, Thomann A-L, Bauchire J-M. AlCoCrCuFeNi high entropy alloy cluster growth and annealing on silicon: a classical molecular dynamics simulation study. Appl Surf Sci 2013;285:810–16. doi:10.1016/j.apsusc.2013.08.133.

[32] Xie L, Brault P, Thomann A-L, Yang X, Zhang Y, Shang G. Molecular dynamics simulation of Al–Co–Cr–Cu–Fe–Ni high entropy alloy thin film growth. Intermetallics 2016;68:78–86. doi:10.1016/j.intermet.2015.09.008.

[33] Tong C-J, Chen Y-L, Yeh J-W, Lin S-J, Chen S-K, Shun T-T, et al. Microstructure characterization of Al_xCoCrCuFeNi high-entropy alloy system with multiprincipal elements. Metall Mater Trans A 2005;36(4):881–93. doi:10.1007/s11661-005-0283-0.

[34] Tsai M-H, Yeh J-W. High-entropy alloys: a critical review. Mater Res Lett 2014;2(3):107–23. doi:10.1080/21663831.2014.912690.

[35] Yu C, Xu X, Chen M, Liu C. Atomistic mechanism of nano-scale phase separation in fcc-based high entropy alloys. J Alloy Compd 2016;663:340–4. doi:10.1016/j.jallcom.2015.12.004.

[36] Xu X, Liu P, Guo S, Hirata A, Fujita T, Nieh T, et al. Nanoscale phase separation in a fcc-based CoCrCuFeNiAl$_{0.5}$ high-entropy alloy. Acta Mater 2015;84:145–52. doi:10.1016/j.actamat.2014.10.033.
[37] Wang F, Zhang Y, Chen G, Davies HA. Tensile and compressive mechanical behavior of a CoCrCuFeNiAl$_{0.5}$ high entropy alloy. Int J Modern Phys B 2009;23(06n07):1254–9. doi:10.1142/S0217979209060774.
[38] Singh S, Wanderka N, Murty B, Glatzel U, Banhart J. Decomposition in multicomponent AlCoCrCuFeNi high-entropy alloy. Acta Mater 2011;59(1):182–90. doi:10.1016/j.actamat.2010.09.023.
[39] Pickering E, Stone H, Jones N. Fine-scale precipitation in the high-entropy alloy Al$_{0.5}$CrFeCoNiCu. Mater Sci Eng 2015;645:65–71. doi:10.1016/j.msea.2015.08.010.
[40] Nadutov V, Makarenko SY, Volosevich PY. Effect of aluminum on fine structure and distribution of chemical elements in high-entropy alloys Al$_x$ FeNiCoCuCr. Phys Met Metallogr 2015;116(5):439–44. doi:10.1134/S0031918X15030096.
[41] Wu J-M, Lin S-J, Yeh J-W, Chen S-K, Huang Y-S, Chen H-C. Adhesive wear behavior of Al$_x$ CoCrCuFeNi high-entropy alloys as a function of aluminum content. Wear 2006;261(5):513–19. doi:10.1016/j.wear.2005.12.008.
[42] Roy U, Roy H, Daoud H, Glatzel U, Ray K. Fracture toughness and fracture micromechanism in a cast AlCoCrCuFeNi high entropy alloy system. Mater Lett 2014;132:186–9. doi:10.1016/j.matlet.2014.06.067.
[43] Hemphill MA, Yuan T, Wang G, Yeh J, Tsai C, Chuang A, et al. Fatigue behavior of Al$_{0.5}$ CoCrCuFeNi high entropy alloys. Acta Mater 2012;60(16):5723–34. doi:10.1016/j.actamat.2012.06.046.
[44] Tsai C-W, Chen Y-L, Tsai M-H, Yeh J-W, Shun T-T, Chen S-K. Deformation and annealing behaviors of high-entropy alloy Al$_{0.5}$ CoCrCuFeNi. J AlloyCompd 2009;486(1):427–35. doi:10.1016/j.jallcom.2009.06.182.
[45] Guo S, Ng C, Lu J, Liu C. Effect of valence electron concentration on stability of fcc or bcc phase in high entropy alloys. JApplPhys 2011;109(10):103505. doi:10.1063/1.3587228.
[46] Kuznetsov A, Shaysultanov D, Stepanov N, Salishchev G, Senkov O. Tensile properties of an AlCrCuNiFeCo high-entropy alloy in as-cast and wrought conditions. Mater Sci Eng 2012;533:107–18. doi:10.1016/j.msea.2011.11.045.
[47] Zhang K, Pan S, Tang W, Zhang Y, Wei B. Structural and bonding transformation of al0. 67CrCoCuFeNi high-entropy alloys during quenching. J Alloy Compd 2018;753:636–41. doi:10.1016/j.jallcom.2018.04.252.
[48] Tong C-J, Chen Y-L, Yeh J-W, Lin S-J, Chen S-K, Shun T-T, et al. Microstructure characterization of al x cocrcufeni high-entropy alloy system with multiprincipal elements. Metall Mater Trans A 2005;36(4):881–93. doi:10.1007/s11661-005-0283-0.
[49] Miracle DB, Senkov ON. A critical review of high entropy alloys and related concepts. Acta Mater 2017;122:448–511. doi:10.1016/j.actamat.2016.08.081.
[50] Tsai K-Y, Tsai M-H, Yeh J-W. Sluggish diffusion in Co–Cr–Fe–Mn–Ni high-entropy alloys. Acta Mater 2013;61(13):4887–97. doi:10.1016/j.actamat.2013.04.058.
[51] Zhang Y, Chen Z, Cao D, Zhang J, Zhang P, Tao Q, et al. Concurrence of spinodal decomposition and nano-phase precipitation in a multi-component AlCoCrCuFeNi high-entropy alloy. J Mater Res Technol 2019;8(1):726–36. doi:10.1016/j.jmrt.2018.04.020.
[52] Hao Z, Cui R, Fan Y, Lin J. Diffusion mechanism of tools and simulation in nanoscale cutting the Ni–Fe–Cr series of nickel-based superalloy. Int J Mech Sci 2019;150:625–36. doi:10.1016/j.ijmecsci.2018.10.058.
[53] Korchuganov A, Lutsenko I. Molecular dynamics research of mechanical, diffusion and thermal properties of CoCrFeMnNi high-entropy alloys. In: AIP conference proceedings, 2053. AIP Publishing; 2018. p. 40046. doi:10.1063/1.5084484.
[54] Ding J, Asta M, Ritchie RO. Melts of CrCoNi-based high-entropy alloys: atomic diffusion and electronic/atomic structure from ab initio simulation. Appl Phys Lett 2018;113(11):111902. doi:10.1063/1.5045216.
[55] Sharma A, Singh P, Johnson DD, Liaw PK, Balasubramanian G. Atomistic clustering-ordering and high-strain deformation of an Al$_{0.1}$ CrCoFeNi high-entropy alloy. Sci Rep 2016;6. doi:10.1038/srep31028.
[56] Tang C, Ren P, Chen X. Cooling of Al-Cu-Fe-Cr-Ni high entropy alloy with different size. Phys Lett A 2019;383(19):2290–5. doi:10.1016/j.physleta.2019.03.031.
[57] Sharma A, Deshmukh SA, Liaw PK, Balasubramanian G. Crystallization kinetics in AlxCrCoFeNi (0 x 40) high-entropy alloys. Scr Mater 2017;141:54–7. doi:10.1016/j.scriptamat.2017.07.024.
[58] Li Y, Lv M, Liang H. Molecular dynamics study of local structure evolution of AlCrCoCuFeNi high entropy alloy in rapidly cooled process. J Comput Theor Nanosci 2015;12(11):4649–53. doi:10.1166/jctn.2015.4413.
[59] Li J, Fang Q, Liu B, Liu Y, Liu Y. Mechanical behaviors of AlCrFeCuNi high-entropy alloys under uniaxial tension via molecular dynamics simulation. RSC Adv 2016;6(80):76409–19. doi:10.1039/c6ra16503f.
[60] Li J, Fang Q, Liu B, Liu Y. Transformation induced softening and plasticity in high entropy alloys. Acta Mater 2018;147:35–41. doi:10.1016/j.actamat.2018.01.002.
[61] Fang Q, Chen Y, Li J, Jiang C, Liu B, Liu Y, et al. Probing the phase transformation and dislocation evolution in dual-phase high-entropy alloys. Int J Plast 2019;114:161–73. doi:10.1016/j.ijplas.2018.10.014.
[62] Afkham Y, Bahramyan M, Mousavian RT, Brabazon D. Tensile properties of AlCrCoFeCuNi glassy alloys: amolecular dynamics simulation study. Mater Sci Eng 2017;698:143–51. doi:10.1016/j.msea.2017.05.057.
[63] Daw MS, Foiles SM, Baskes MI. The embedded-atom method: a review of theory and applications. Mater Sci Rep 1993;9(7):251–310. doi:10.1016/0920-2307(93)90001-U.
[64] Zhou X, Johnson R, Wadley H. Misfit-energy-increasing dislocations in vapor-deposited cofe/nife multilayers. Physical Review B 2004;69(14):144113. doi:10.1103/PhysRevB.69.144113.
[65] Plimpton S. Fast parallel algorithms for short-range molecular dynamics. JComputPhys 1995;117(1):1–19. doi:10.1006/jcph.1995.1039.
[66] Stukowski A. Visualization and analysis of atomistic simulation data with ovito–the open visualization tool. Model Simul Mater Sci Eng 2009;18(1):15012. doi:10.1088/0965-0393/18/1/015012.
[67] Faken D, Jónsson H. Systematic analysis of local atomic structure combined with 3D computer graphics. Comput Mater Sci 1994;2(2):279–86. doi:10.1016/0927-0256(94)90109-0.
[68] Tsuzuki H, Branicio PS, Rino JP. Structural characterization of deformed crystals by analysis of common atomic neighborhood. ComputPhysCommun 2007;177(6):518–23. doi:10.1016/j.cpc.2007.05.018.
[69] Coleman S, Spearot D, Capolungo L. Virtual diffraction analysis of Ni [0 1 0] symmetric tilt grain boundaries. Model Simul Mater Sci Eng 2013;21(5):55020. doi:10.1088/0965-0393/21/5/055020.
[70] Peng L-M, Ren G, Dudarev S, Whelan M. Robust parameterization of elastic and absorptive electron atomic scattering factors. Acta Crystallogr Sect A 1996;52(2):257–76. doi:10.1107/S0108767395014371.
[71] Diao H, Santodonato LJ, Tang Z, Egami T, Liaw PK. Local structures of high-entropy alloys (heas) on atomic scales: an overview. JOM 2015;67(10):2321–5. doi:10.1007/s11837-015-1591-5.
[72] Owen L, Pickering E, Playford H, Stone HJ, Tucker M, Jones NG. An assessment of the lattice strain in the CrMnFeCoNi high-entropy alloy. Acta Mater 2017;122:11–18. doi:10.1016/j.actamat.2019.02.038.
[73] Tung C-C, Yeh J-W, Shun T, Chen S-K, Huang Y-S, Chen H-C. On the elemental effect of AlCoCrCuFeNi high-entropy alloy system. MaterLett 2007;61(1):1–5. doi:10.1016/j.matlet.2006.03.140.
[74] Yeh J-W, Chen S-K, Lin S-J, Gan J-Y, Chin T-S, Shun T-T, et al. Nanostructured high-entropy alloys with multiple principal elements: novel alloy design concepts and outcomes. Adv Eng Mater 2004;6(5):299–303. doi:10.1002/adem.200300567.
[75] Li J, Chen H, Li S, Fang Q, Liu Y, Liang L, et al. Tuning the mechanical behavior of high-entropy alloys via controlling cooling rates. Mater Sci Eng 2019;760:359–65. doi:10.1016/j.msea.2019.06.017.
[76] Li C, Zhao M, Li J, Jiang Q. B 2 structure of high-entropy alloys with addition of al. J Appl Phys 2008;104(11):113504. doi:10.1063/1.3032900.
[77] Bönisch M, Wu Y, Sehitoglu H. Twinning-induced strain hardening in dual-phase FeCoCrNiAl 0.5 at room and cryogenic temperature. SciRep 2018;8. doi:10.1038/s41598-018-28784-1.
[78] Sheng H, Ma E, Kramer MJ. Relating dynamic properties to atomic structure in metallic glasses. JOM 2012;64(7):856–81. doi:10.1007/s11837-012-0360-y.
[79] Duan G, Xu D, Zhang Q, Zhang G, Cagin T, Johnson WL, et al. Molecular dynamics study of the binary Cu$_{46}$ Zr$_{54}$ metallic glass motivated by experiments: glass formation and atomic-level structure. Phys Rev B 2005;71(22):224208. doi:10.1103/PhysRevB.71.224208.
[80] Gao M, Alman D. Searching for next single-phase high-entropy alloy compositions. Entropy 2013;15(10):4504–19. doi:10.3390/e15104504.
[81] Feng X, Zhang J, Wu K, Liang X, Liu G, Sun J. Ultrastrong al 0.1 cocrfeni high-entropy alloys at small scales: effects of stacking faults vs. nanotwins. Nanoscale 2018;10(28):13329–34. doi:10.1039/c8nr03573c.